

Correlation-driven chiral superconductivity and chiral spin order in doped kagome lattice

Shun-Li Yu and Jian-Xin Li

National Laboratory of Solid State Microstructures and Department of Physics, Nanjing University, Nanjing 210093, China
(Dated: November 1, 2011)

We study the electronic instabilities of the Hubbard model in the $1/6$ hole-doped Kagome lattice using the variational cluster approach. The $1/6$ hole doping is unique in the sense that the Fermi level is at the von Hove singularity and the Fermi surface has a perfect nesting. In this case, a density wave is usually realized. However, we demonstrate here that the chiral $d_{x^2-y^2} + id_{xy}$ superconducting state is most favorable when a small Hubbard interaction U ($U < 3.0t$) is introduced, and a scalar *chiral* spin order is realized at large U ($U > 5.0t$). Between them, a spin-disordered insulating state is proposed.

PACS numbers: 74.20.-z, 75.10.-b, 71.10.-w, 71.27.+a

The kagome lattice has recently attracted considerable interest due to its higher degree of frustration. Several possible states have been proposed for the Heisenberg model in this lattice, including the $U(1)$ algebraic spin liquid (SL) [1], the valence bond solid [2], and the gapped SL [3]. Recently, the numerical study shows that its ground state is a singlet-gapped SL with signatures of Z_2 topological order [4]. On the other hand, the anomalous quantum Hall effect [5] and the topological insulator [6] have also been demonstrated to exist when the electron filling is near the Dirac point at $2/3$ electron density. In view of the rapid developments in the investigation of these exotic quantum phases, the question arises if other correlation-driven exotic quantum orders will be realized when the system is doped away from half-filling. We note that the Fermi level is at the von Hove singularity and the Fermi surface (FS) has a perfect nesting at $1/6$ hole doping. By using the variational cluster approach (VCA) to the Hubbard model in the kagome lattice, we show that a chiral $d_{x^2-y^2} + id_{xy}$ superconducting (SC) order and a non-coplanar chiral spin density wave (SDW) can be realized at the $1/6$ hole doping.

Chiral superconductivity and chiral magnetic order are two distinctive phases of matter. They break both the time-reversal symmetry and the parity symmetry. The nontrivial topology of them can result in a wealth of fascinating properties, such as spontaneous quantum Hall effect [7, 8], unusual magnetoelectric properties [9], and a quantized boundary current in magnetic field [10]. Experimentally, the spin-triplet p -wave chiral superconductivity has been found in Sr_2RuO_4 [11]. And, the chiral spin order was proposed to describe the magnetic ordering in Mn monolayers on Cu(111) surfaces [12] and the nuclear spin ground state of a two-dimensional solid ^3He [13]. Recently, the chiral spin order was also proposed in the doped triangular lattice [14], the pyrochlore lattice [15] and the doped graphene [16] based on the mean-field analysis. In particular, the renormalization group calculations [17, 18] show that the chiral $d_{x^2-y^2} + id_{xy}$ superconductivity is favored in the doped

graphene with a perfect FS nesting. Here, we show that both the $d_{x^2-y^2} + id_{xy}$ superconducting order and a non-coplanar chiral SDW order can be realized in the $1/6$ hole-doped kagome lattice by tuning the on-site Coulomb interaction U .

The Hubbard model in the kagome lattice is defined as

$$H = -t \sum_{\langle ij \rangle \sigma} (c_{i\sigma}^\dagger c_{j\sigma} + h.c.) + U \sum_i n_{i\uparrow} n_{i\downarrow}, \quad (1)$$

where $c_{i\sigma}^\dagger$ ($c_{i\sigma}$) creates (annihilates) an electron with spin σ on site i and $n_{i\sigma} = c_{i\sigma}^\dagger c_{i\sigma}$, $\langle \cdots \rangle$ denotes the nearest-neighbor (NN) bond. Each unit cell of the kagome lattice contains three sites (labeled by α , β and γ in Fig.1(a)). Except for a flat band at the top of the energy band, the two dispersive bands are the same as those in the honeycomb lattice (Fig.1(b)). From the density of states shown in Fig.1(d), one can see that there are three von Hove singularities at $-2t$, 0 and $2t$. That at $2t$ originates from the flat band, the other two originate from the saddle points at M point (see Fig.1(b)). The Fermi levels at $-2t$ and 0 correspond to the $1/2$ and $1/6$ hole doping. In two cases, the FS forms a hexagon and displays a perfect nesting (see Fig.1(c)). As the correlation effect at $1/2$ doping is much weaker than that at $1/6$ doping, we focus our study on the $1/6$ hole doping here.

VCA is a cluster approximation of the self-energy functional approach [19], which uses the rigorous variational principle $\delta\Omega(\Sigma)/\delta\Sigma = 0$ for the thermodynamic grand potential Ω to determine the physical self-energy Σ . It has been successfully applied to the problem of competing phases in many strong correlation systems [20–23]. In VCA, the lattice is tiled into identical clusters, which make up of a reference system with the same two-body interaction as the original system but a different one-body part (including the added Weiss fields to study the symmetry broken phases). Then the exact Green function G' (and the self-energy Σ') for each cluster is calculated by exact diagonalization method. So, the short-range static and dynamical (within each cluster) correlations

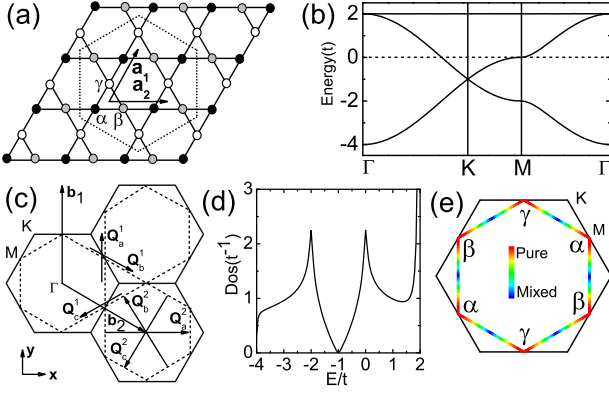


FIG. 1: (color online) (a) Structure of kagome lattice and the 12-site cluster tiling (enclosed by dotted lines) used in our VCA calculation. \mathbf{a}_1 and \mathbf{a}_2 are the lattice unit vectors. (b) The tight-binding dispersion along high symmetric directions (as illustrated in (c)). The dashed line is the Fermi level corresponding to the 1/6 hole doping. (c) The Brillouin zone and FS for the 1/6 hole doping. \mathbf{b}_1 and \mathbf{b}_2 are the reciprocal-lattice vectors. The dashed lines denote the FS and the vectors $\mathbf{Q}_{a,b,c}^{1,2}$ are the nesting vectors. (d) Density of state. (e) Weights of the contribution to FS from three inequivalent lattice sites α , β and γ as represented by the colors.

have been taken into account precisely. For any Σ' parameterized as $\Sigma'(\mathbf{t}')$, where \mathbf{t}' represents the collection of the one-body terms, we have the grand potential [19]:

$$\Omega[\Sigma'(\mathbf{t}')] = \Omega'(\mathbf{t}') + \text{Tr} \ln[-G'(\mathbf{t}')] - \text{Tr} \ln[-G(\mathbf{t}')], \quad (2)$$

where $\Omega'(\mathbf{t}')$ is the grand potential of the reference system and $G(\mathbf{t}')$ is the approximate Green function of the original system calculated through the cluster perturbation theory [24]. Eq.(2) is no longer a functional but an ordinary function of the variational parameters \mathbf{t}' , and the task of VCA is to find a stationary point of this function, $\partial\Omega(\mathbf{t}')/\partial\mathbf{t}' = 0$. In our calculation, the 12-site clusters (as enclosed by the dotted lines in Fig.1(a)) and the open boundary conditions for the clusters are used.

Before presenting our numerical results, let us first discuss the possible SC symmetries at 1/6 hole doping. We note that at each saddle point M the site-contribution to FS comes only from one of the three inequivalent lattice sites, as shown in Fig.1(e). Considering the effect of the van Hove singularity at M -point, it is expected that the favorable Cooper pairings will be made from two electrons belonging to the same sublattice. For the kagome lattice, there are six coordinates in the same sublattice for each site (Fig.1(a)), and it gives rise to three different bonds. Considering that the pairing intensities are the same along all bonds, and the phase differences θ and ϕ with respect to that along the \mathbf{a}_2 direction exists for the other two directions, we will get the following pairing functions: (i) $\Delta(\mathbf{k}) = \cos(k_x) + e^{i\theta} \cos(k_x/2 + \sqrt{3}k_y/2) + e^{i\phi} \cos(k_x/2 - \sqrt{3}k_y/2)$ for the spin-singlet pairing, (ii) $\Delta(\mathbf{k}) = \sin(k_x) + e^{i\theta} \sin(k_x/2 +$

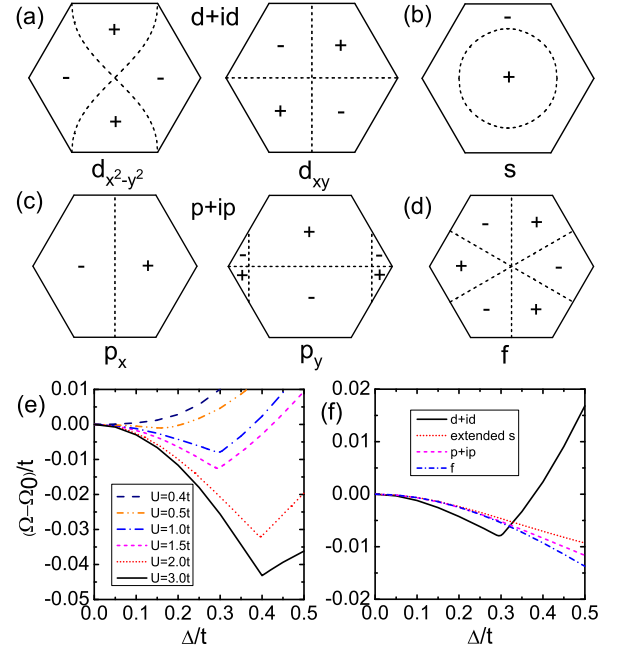


FIG. 2: (color online) (a)-(d) Phase(\pm) of the SC gap functions for the four possible pairing symmetries. The dotted lines denote the gap nodes. (e) Scaled grand potential Ω as a function of Weiss field Δ for different U in the $d_{x^2-y^2} + id_{xy}$ channel. (f) Scaled Ω as a function of Δ for different pairing symmetries at $U = t$.

$\sqrt{3}k_y/2) + e^{i\phi} \sin(k_x/2 - \sqrt{3}k_y/2)$ for the spin-triplet pairing. The most natural choices for the phases are $(\theta, \phi) = (0, 0)$ and $(2\pi/3, -2\pi/3)$. So, we have: (i) the $d_{x^2-y^2} + id_{xy}$ wave for $(\theta, \phi) = (2\pi/3, -2\pi/3)$, $\Delta^{d+id}(\mathbf{k}) = \Delta_0[\cos(k_x) - \cos(k_x/2)\cos(\sqrt{3}k_y/2) + i\sqrt{3}\sin(k_x/2)\sin(\sqrt{3}k_y/2)]$; (ii) the extended s wave for $(\theta, \phi) = (0, 0)$, $\Delta^s(\mathbf{k}) = \Delta_0[\cos(k_x) + 2\cos(k_x/2)\cos(\sqrt{3}k_y/2)]$; (iii) the $p_x + ip_y$ wave for $(\theta, \phi) = (2\pi/3, -2\pi/3)$, $\Delta^{p+ip}(\mathbf{k}) = \Delta_0[\sin(k_x) - \sin(k_x/2)\cos(\sqrt{3}k_y/2) + i\sqrt{3}\cos(k_x/2)\sin(\sqrt{3}k_y/2)]$; and (iv) the f wave for $(\theta, \phi) = (0, 0)$, $\Delta^f(\mathbf{k}) = \Delta_0[\sin(k_x) + 2\sin(k_x/2)\cos(\sqrt{3}k_y/2)]$. The phases and the gap nodes for the four pairing symmetries are shown in Fig.2(a)-(d).

With the above pairing functions, we now introduce the Weiss fields $H' = \Delta \sum_{\langle\langle ij \rangle\rangle} e^{i\theta_{ij}} \Delta_{ij}^{s/t} + h.c.$, where $\Delta_{ij}^{s/t} = c_{i\uparrow}c_{j\downarrow} \mp c_{i\downarrow}c_{j\uparrow}$ for the singlet/triplet pairing, to test the possible pairing orders. Here, $\langle\langle \cdot \cdot \rangle\rangle$ denotes the bonds linking the sites in the same sublattice and θ_{ij} is given according to the rule discussed above. Fig.2(e) presents the results of $\Omega - \Omega_0$ as a function of Δ for the $d_{x^2-y^2} + id_{xy}$ pairing symmetry at various U . Ω_0 is the grand potential in the zero Weiss field. For $0.4t < U < 3t$, we find that there is a minimum at finite Δ , at the same time it satisfies $\partial\Omega(\Delta)/\partial\Delta = 0$. For $U \leq 0.4t$, a monotonic increase with Δ occurs. While, though there is also a minimum at finite Δ for $U \geq 3t$,

we find that the derivative at this minimum does not exist, because Ω is not smooth at the point. Thus, it is not a stationary point of the self-energy functional, according to the variational principle of VCA [19]. So, the $d_{x^2-y^2} + id_{xy}$ pairing order is realized only in the region $0.4t < U < 3t$. We have also checked the stationarity of other three SC pairing orders. The typical results are shown in Fig.2(f) for $U = t$. Except for the $d_{x^2-y^2} + id_{xy}$ pairing, all other three pairings exhibit a monotonic decrease with the Weiss field. Therefore, they are not stable solutions.

In the system with a perfect nesting FS, one will expect naturally an instability to the density wave which may compete with the SC order. In the presence of the on-site Hubbard U , the most likely density wave would be a SDW. A well known example is that the staggered SDW order occurs for the half-filled Hubbard model with a perfect FS nesting in the square lattice, where the nesting wave vector $(\pm\pi, \pm\pi)$ coincides exactly the real-space translation symmetry of two unit distances for the staggered SDW. Considering the geometry of the kagome lattice and consequently the nesting property for the 1/6 hole doping as shown in Fig.1(c), the staggered SDW will not be favored here. Then, what is the kagome-lattice counterpart of the staggered SDW occurring on the half-filled square lattice? At 1/6 hole doping, the nesting FS has the nesting vectors $\mathbf{Q}_{a,b,c}^2$ (or $\mathbf{Q}_{a,b,c}^1$ which connects to $\mathbf{Q}_{a,b,c}^2$ via the reciprocal-lattice vectors) as indicated in Fig.1(c). With these nesting vectors, two distinct magnetic orders are expected. One is the non-coplanar chiral spin order associated with $\mathbf{Q}_{a,b,c}^1$ as shown in Fig.1(c), which is similar to that proposed in the doped triangle [14] and honeycomb [16] lattices, where the four local spins direct along the normals to the faces of a regular tetrahedron (Fig.3). Thus, the spin orientations are: $\mathbf{e}_{i\alpha} = 1/\sqrt{3}[\mathbf{e}_x \cos(\mathbf{Q}_a^1 \cdot \mathbf{R}_i) + \mathbf{e}_y \cos(\mathbf{Q}_b^1 \cdot \mathbf{R}_i) + \mathbf{e}_z \cos(\mathbf{Q}_c^1 \cdot \mathbf{R}_i)]$, $\mathbf{e}_{i\beta} = 1/\sqrt{3}[\mathbf{e}_x \cos(\mathbf{Q}_a^1 \cdot \mathbf{R}_i) - \mathbf{e}_y \cos(\mathbf{Q}_b^1 \cdot \mathbf{R}_i) - \mathbf{e}_z \cos(\mathbf{Q}_c^1 \cdot \mathbf{R}_i)]$ and $\mathbf{e}_{i\gamma} = 1/\sqrt{3}[-\mathbf{e}_x \cos(\mathbf{Q}_a^1 \cdot \mathbf{R}_i) - \mathbf{e}_y \cos(\mathbf{Q}_b^1 \cdot \mathbf{R}_i) + \mathbf{e}_z \cos(\mathbf{Q}_c^1 \cdot \mathbf{R}_i)]$, where \mathbf{R}_i denotes the position of the unit cell i . In this state, the resulting scalar spin chirality, $\langle K_s \rangle = \langle \mathbf{S}_\alpha \cdot (\mathbf{S}_\beta \times \mathbf{S}_\gamma) \rangle \neq 0$ in each triangular plaquette, breaks both the time-reversal and the parity symmetries. The other is the coplanar vector chiral spin order associated with $\mathbf{Q}_{a,b,c}^2$, as shown in Fig.3(b). In this case, the spins in each triangular plaquette orient at 120° to each other. The vector chirality for each triangle can be defined as $\mathbf{K}_v = (2/3\sqrt{3})(\mathbf{S}_\alpha \times \mathbf{S}_\beta + \mathbf{S}_\beta \times \mathbf{S}_\gamma + \mathbf{S}_\gamma \times \mathbf{S}_\alpha)$, which is parallel to the z axis with amplitude $+1$ or -1 . As shown in Fig.3(b), the vector chirality arranges as a “stripe” phase, in which each chirality arranges in a stripe and the two stripes are staggered with each other. The scalar chiral spin order and the vector chiral spin order have different translational symmetries in real space as indicated in Fig.3(a) and (b), where the magnetic translation vectors are shown as the dotted lines.

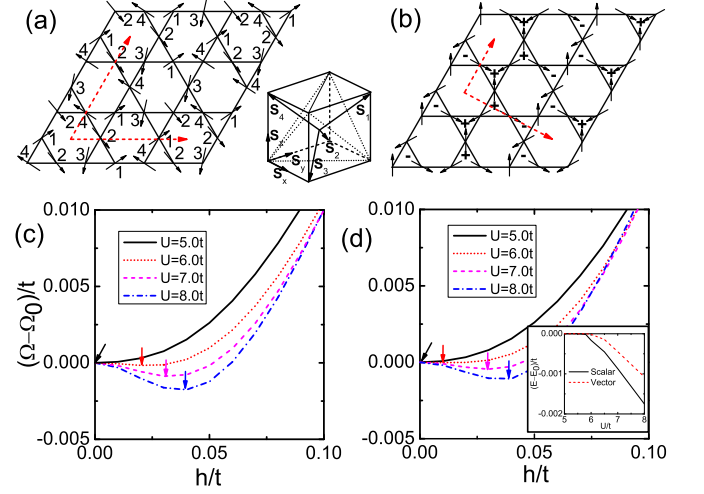


FIG. 3: (color online) (a) Non-coplanar arrangement of spins (scalar spin chirality). $\mathbf{S}_{1 \rightarrow 4}$ indicate the four directions of local magnetic moments. (b) Coplanar arrangement of spins (vector spin chirality). The dashed lines with arrow in (a) and (b) are the magnetic translation vectors. (c) Scaled grand potential Ω as a function of the Weiss field h for the spin order shown in (a) at various U . The local minima are indicated by arrows. (d) Scaled Ω as a function of h for the spin order shown in (b). The inset of (d) shows the energy differences between the two spin ordered states and the normal phase with a zero Weiss field, respectively.

To test the favorable SDW, we introduce the following Weiss field: $H' = h \sum_{i\eta} \mathbf{e}_{i\eta} \cdot \mathbf{S}_{i\eta}$, where $\mathbf{e}_{i\eta}$ is the orientation of magnetic moment and $\mathbf{S}_{i\eta} = \sum_{\sigma\sigma'} c_{i\eta\sigma}^\dagger \boldsymbol{\tau}_{\sigma\sigma'} c_{i\eta\sigma'}$ with $\boldsymbol{\tau}$ the Pauli matrixes, i the unit cell index and η the site index. Fig.3(c) and (d) show the results for $\Omega - \Omega_0$ as a function of the Weiss field h for the scalar chiral spin order and the vector chiral spin order, respectively. We find that a local minimum exists only for $U > 5.5t$ in both cases. Therefore, in the region $0.4t < U < 3t$, no SDW state will compete with the chiral $d_{x^2-y^2} + id_{xy}$ pairing state. Fig.3(c) and (d) show that both spin ordering states are more favorable compared to the spin disordered state. So, we need to compare their energy gain which is given by the energy difference between the ordered solution and the normal solution found by suppressing the Weiss fields. The energy density $E = \Omega + \mu n$ as a function of electron density n can be obtained for a solution with the functional Ω . The calculation of the energy gain is performed for several values of the chemical potential μ until the density n is close enough to 1/6 doping, and the cluster's chemical potential μ' is also used as a variational parameter to guarantee the thermodynamic consistency [21]. The inset of Fig.3(d) shows the energy gain for the two spin ordered solutions as a function of U . It shows that the scalar chiral spin order state is more favorable than the vector chiral spin order state for $U > 5.5t$. With decreasing U , the difference of the energy gain for the two spin-ordered states decreases.

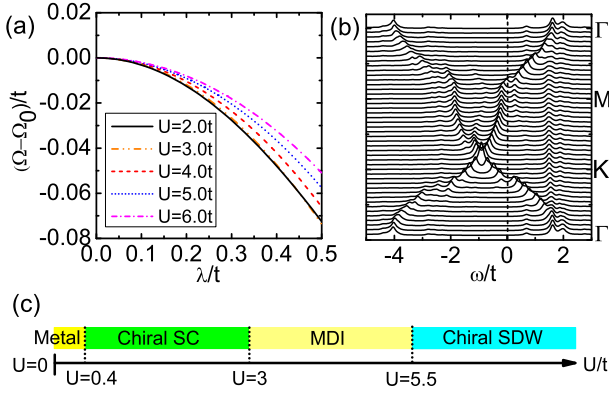


FIG. 4: (color online) (a) Scaled grand potential Ω as a function of Weiss field λ for the conventional CDW order (see text) at various U . (b) Spectral functions for $U = 4t$ along the high symmetric directions (see Fig.1(c)). (c) Qualitative phase diagram of the Hubbard model in the kagome lattice for 1/6 hole doping.

Near the threshold U for the occurrence of the spin order states, the two states are nearly degenerate.

To check the possible existence of the charge-density wave (CDW) in this system, $H' = \lambda \sum_i (f_\alpha n_{i\alpha} \cos(\mathbf{Q}_\alpha^1 \cdot \mathbf{r}_i) + f_\beta n_{i\beta} \cos(\mathbf{Q}_\beta^1 \cdot \mathbf{r}_i) + f_\gamma n_{i\gamma} \cos(\mathbf{Q}_\gamma^1 \cdot \mathbf{r}_i))$ is used, with i the unit cell index and $(f_\alpha, f_\beta, f_\gamma) = (1, 0, -1)$. The dependence of $\Omega - \Omega_0$ on the Weiss field λ is presented in Fig.4(a). We find that $\Omega - \Omega_0$ decreases monotonously with λ for various U from $U = 2 \sim 6t$. Therefore, the CDW does not exist in this region. Thus, in the region $0.4t < U < 3t$, the only stable state we found is the chiral $d_{x^2-y^2} + id_{xy}$ pairing state, while for $U > 5.5t$ the most favorable state is the scalar chiral spin order state. In the region between them, we do not find evidence of the SC state, spin order state and the CDW state. From the spectral function of single-particle excitations, we find that a gap occurs at the Fermi level as presented in Fig.4(b) for $U = 4t$ (a non-vanishing spectral weight can be seen in the gapped region because a finite Lorentzian broadening is used in the numerical calculations). So, the system is in fact an insulator. We would suggest that the system is a magnetic disordered insulator (MDI). The possible candidates may be the spin liquid, the spin glass or the valence-bond solid, but the method used here can not identify or distinguish them.

Finally, we summarize the results obtained above in the phase diagram shown in Fig.4(c). We note that the spin-1/2 kagome lattice has been realized in Herbertsmithite $\text{ZnCu}_3(\text{OH})_6\text{Cl}_2$ [25, 26] and its isostructural Mg-based paracatamite $\text{MgCu}_3(\text{OH})_6\text{Cl}_2$ [27]. Also, the kagome lattice has been simulated experimentally in ultra-cold atoms [28]. So, we suggest that the theoretical predictions presented here may be probed after doping these compounds or by implementing an optical lattice in ultra-cold atoms where the Hubbard interaction U can

be tuned continuously.

In summary, we have studied the Hubbard model in the 1/6 hole doped kagome lattice using the variational cluster approach. We find that the chiral $d_{x^2-y^2} + id_{xy}$ superconducting state is most favorable at a small Hubbard interaction U ($0.4t < U < 3t$), and the scalar chiral spin order is realized at the large U ($U > 5.5t$). Between them, a magnetic disordered insulating state is proposed.

We thank F. Wang and Q. H. Wang for helpful discussions, in particular F. Wang for pointing out Ref.[17]. This work was supported by the National Natural Science Foundation of China (10525415) and the Ministry of Science and Technology of China (973 project Grants Nos.2006CB601002,2006CB921800).

-
- [1] Y. Ran, M. Hermele, P. A. Lee, and X. G. Wen, Phys. Rev. Lett. **98**, 117205 (2007).
 - [2] R. R. P. Singh, and D. A. Huse, Phys. Rev. B **76**, 18407 (2007).
 - [3] H. C. Jiang, Z. Y. Weng, D. N. Sheng, Phys. Rev. Lett. **101**, 117203 (2008).
 - [4] S. Yan, D. A. Huse, S. R. White, Science **332**, 1173 (2011).
 - [5] S. L. Yu, J. X. Li, and L. Sheng, Phys. Rev. B **80**, 193304 (2009).
 - [6] H. M. Guo, and M. Franz, Phys. Rev. B **80**, 113102 (2009).
 - [7] B. Horovitz, and A. Golub, Phys. Rev. B **68**, 214503 (2003).
 - [8] K. Ohgushi, S. Murakami, and N. Nagaosa, Phys. Rev. B **62**, 6065 (2000).
 - [9] L. N. Bulaevskii and C. D. Batista, M. V. Mostovoy, and D. I. Khomskii, Phys. Rev. B **78**, 024402 (2008).
 - [10] R. B. Laughlin, Phys. Rev. Lett. **80**, 5188 (1998).
 - [11] A. P. Mackenzie and Y. Maeno, Rev. Mod. Phys. **75**, 657 (2003).
 - [12] Ph. Kurz, G. Bihlmayer, K. Hirai, and S. Blügel, Phys. Rev. Lett. **86**, 1106 (2001).
 - [13] T. Momoi, K. Kubo, and K. Niki, Phys. Rev. Lett. **79**, 2081 (1997).
 - [14] I. Martin and C. D. Batista, Phys. Rev. Lett. **101**, 156402 (2008).
 - [15] G. W. Chern, Phys. Rev. Lett. **105**, 226403 (2010).
 - [16] T. Li, arXiv:1103.2420 (2011).
 - [17] R. Nandkishore, L. S. Levitov, and A. V. Chubukov, arXiv:1107.1903 (2011).
 - [18] W. S. Wang, Y. Y. Xiang, Q. H. Wang, F. Wang, F. Yang, and D. H. Lee, arXiv:1109.3884 (2011).
 - [19] M. Potthoff, Eur. Phys. J. B **32**, 429 (2003); M. Potthoff, M. Aichhorn, and C. Dahnken, Phys. Rev. Lett. **91**, 206402 (2003).
 - [20] D. Sénéchal, P.-L. Lavertu, M.-A. Marois, and A.-M. S. Tremblay, Phys. Rev. Lett. **94**, 156404 (2005).
 - [21] M. Aichhorn, E. Arrigoni, M. Potthoff, and W. Hanke, Phys. Rev. B **74**, 024508 (2006).
 - [22] P. Sahebsara, and D. Sénéchal, Phys. Rev. Lett. **97**, 257004 (2006).
 - [23] S. L. Yu, X. C. Xie, and J. X. Li, Phys. Rev. Lett. **107**,

- 010401 (2011).
- [24] D. Sénéchal, and A.-M. S. Tremblay, Phys. Rev. Lett. **92**, 126401 (2004).
- [25] M. P. Shores, E. A. Nytko, B. M. Bartlett, and D. G. Nocera, J. Am. Chem. Soc. **127**, 13462 (2005).
- [26] S.-H. Lee, H. Kikuchi, Y. Qiu, B. Lake, Q. Huang, K. Habicht, AND K. Kiefer, Nat. Mater. **6**, 853 (2007).
- [27] E. Kermarrec, P. Mendels, F. Bert, R. H. Colman, A. S. Wills, P. Strobel, P. Bonville, A. Hillier, and A. Amato, Phys. Rev. B **84**, 100401 (2011).
- [28] G. B. Jo, J. Guzman, C. K. Thomas, P. Hosur, A. Vishwanath, and D. M. Stamper-Kurn, arXiv:1109.1591 (2011).